Advances in Water Resources 33 (2010) 1375–1387

Contents lists available at ScienceDirect

Advances in Water Resources

journal homepage: www.elsevier.com/ locate/advwatres

Three-dimensional flow patterns at the river–aquifer interface — a case study at the Danube

J. Derx [a,b,*], A.P. Blaschke [a], G. Blöschl [a,b]

[a] Institute of Hydraulic Engineering and Water Resources Management, Vienna University of Technology, Austria
[b] Centre for Water Resource Systems, Vienna University of Technology, Austria

ARTICLE INFO

Article history:
Received 30 October 2009
Received in revised form 13 April 2010
Accepted 27 April 2010
Available online 26 May 2010

Keywords:
River–aquifer exchange
River–aquifer mixing processes
Morphological formation
Groundwater modelling

ABSTRACT

The three-dimensional groundwater flow patterns in a gravel bar at the Danube east of Vienna were investigated and are discussed in this paper. The observed groundwater level gradients are highly dynamic and respond very quickly to changes in the river water levels. A variably saturated groundwater model was calibrated to the data to describe the complex dynamics of flow in the gravel bar. The model results suggest that short-term (6–48 h) fluctuations of river water levels cause variations in the exchange flow rates from −35 l/s to 82 l/s. The highest rates occur during brief infiltration after rapidly rising river water levels. Simulations of different scenarios indicate that riverbank clogging will decrease the exchange fluxes by up to 80%, while clogging of both riverbank and riverbed essentially stops the flow exchange. The groundwater model is also used to simulate the transport of a conservative tracer. The variation of river water levels over time is shown to increase the extent of the active river–aquifer mixing zone in the gravel bar. These dynamic factors significantly enhance the dilution of conservative tracer concentrations in this zone.

1. Introduction

Surface water–groundwater interaction processes are important for riverine ecological issues, water supply and groundwater management and have been studied at various scales. Studies have investigated the hydraulic connections between streams and aquifers (Fleckenstein et al. [12], Elliott and Brooks [11]). The transport of substances from the surface waters into the aquifers were investigated by various authors (e.g., Mucha et al. [22]), and also the effects of these processes on the fauna, invertebrates and fish eggs (Ingendahl [17], Boulton [4]). On a larger scale, Peyrard et al. [24] showed that floods were influencing the groundwater flow patterns and were able to mimic the strong hydraulic connection between the Garonne river and the adjacent aquifer by a coupled, vertically integrated model. By simulating the dynamic transport of a conservative tracer they found that meandering rivers enhance the exchange at the groundwater–surface water interface. The study site presented in this paper has similar characteristics regarding the magnitude of river discharge and the good hydraulic connection at the river–aquifer interface. The site consists of a gravel bar in the river, which alternates between wet and dry conditions, depending on the river water levels. Because of the geometries of the gravel bar, it was considered likely that the subsurface flow will be three-dimensional. As observed by Peyrard et al. [24] and Lewandowski and Nützmann [19], the groundwater seepage into the river may reverse during rising river water levels leading to infiltration of surface water. These studies, however, did not report on the vertical and lateral extents of the river–aquifer mixing zone and the magnitude of how the exchange rates are affected by this dynamic behaviour. Storey et al. [29] identified the dominant processes controlling the river–aquifer interaction at a riffle–pool sequence in a small stream to be the head difference between the upstream and downstream end of the riffle, the hydraulic conductivity of the sediments and the magnitude of groundwater recharge. They performed steady-state simulations with different input parameters using a three-dimensional groundwater model. They found that the stream stage did not significantly affect the exchange flows, although they did not consider effects of surface water level fluctuations nor factors such as heterogeneous hydraulic aquifer properties and variable geometries of the river banks, such as on gravel bars. Boutt and Fleming [5] found that daily changes in the river water levels due to anthropogenic water releases led to enhanced mass transport and dispersion of a conservative tracer in the near-stream aquifer. They used a 2d groundwater flow and transport model coupled to a simplistic surface water boundary condition for this study. Similarly, a modelling study of Robinson et al. [27] found that tidal forcing induced seawater circulation across the sediment–water interface. These circulation patterns were shown to reduce the concentration of BTEX compounds before their discharge into the sea (Robinson et al. [26]). For the river–aquifer exchange, studies exist on the mixing due to various factors, such as geologic heterogeneities (Fleckenstein et al. [12], Cardenas and Wilson [8], Berkowitz et al. [1]), bed form heterogeneities (Storey et al. [29]) or

* Corresponding author. Institute of Hydraulic Engineering and Water Resources Management, Vienna University of Technology, Austria. Fax: +43 1 58801 22399.
E-mail address: derx@hydro.tuwien.ac.at (J. Derx).

0309-1708/$ – see front matter © 2010 Elsevier Ltd. All rights reserved.
doi:10.1016/j.advwatres.2010.04.013

meandering of rivers (Peyrard et al. [24], Cardenas [7], Boano et al. [3]). The widening of the mixing zone has been observed and simulated for coastal aquifers before (e.g. Lu et al. [20]) and the mechanisms responsible for it have remained a subject of debate. However, to the best of our knowledge, so far no study has investigated the effects of river water fluctuations on the size increase of the mixing zone. We examined the three-dimensional mixing processes at the Danube river, with the focus on the aquifer near the riverbanks. These flow patterns are of importance for the transport of nutrients and for ecological processes. The variation of groundwater velocity magnitudes within the mixing zone due to river water fluctuation could have adverse effects on macrozoobenthos or fish eggs. Furthermore, this paper analyses the mechanisms affecting groundwater response in an aquifer close-by the Austrian Danube. Specifically, the aim of this paper is to understand the effect of short-term (6–48 h) river water fluctuations on the variation of groundwater velocity magnitudes, widening river–aquifer mixing zones and on the dilution of solute concentrations. Moreover, this paper examines to what extent river water fluctuations increase exchange rates between surface water and groundwater.

To address these issues we measured lateral water level gradients in the aquifer close-by the river, which we used to characterise the groundwater flow situation. We then simulated the three-dimensional, variable saturated flow patterns in a gravel bar by a numerical model which we used to estimate the exchange fluxes and flow velocities during groundwater exfiltration–infiltration cycles. We simulated a number of scenarios with different clogging conditions of the riverbed to understand their effect on exchange flow rates. Finally we simulated the transport of a conservative tracer in order to get an appreciation of the spatial distribution of river water penetration depths and the residence times of infiltrated river water in the gravel bar.

2. Test field site and model setup

The study area lies 35 km east of Vienna on the right bank side of the Danube, looking downstream (Fig. 1). It is part of the porous aquifer of the Hainburger Pforte and extends over 1.5 km^2. To the south, the area is bounded by the Hundsheimer Hill and a railway embankment. To the north, the talweg of the Danube has been chosen as a boundary. Most of the landuse in the area is agricultural with a few villages.

A three-dimensional variably saturated groundwater model was setup. The model boundaries are shown in Fig. 1. Within the model domain the hydrogeologic parameters differ greatly between three distinct layers, which consist of a low permeability loamy sand layer on top, a coarse gravel layer and a silty aquitard. The gravel layer outcrops along the river and at the gravel bar. During high water levels the inundated areas adjacent to the river may extend several hundred metres into the floodplain. As a result bank surface conditions alternated between dry and wet during the observation period. The river water levels were recorded at the river gauge (Fig. 1) every 30 min and ranged between the Danube reference low water at Q_{95} and 2.6 m above mean water level with a total water level range of 4.6 m. Q_{95} is hereby defined as the discharge exceeded 95% of the time. For the numerical groundwater flow simulations, time periods during low to mean water were chosen so that the ground surface at the monitoring site never was more than 1.5 m under water (Fig. 2).

2.1. Field observations and data used

At the monitoring site four piezometers (F1, F2, F3 and F4 in Fig. 1) were installed 2 m deep into the ground with perforations for 1.5 m from the bottom. Additionally, one piezometer (F5) was installed 80 m away from the Danube. Groundwater levels were measured manually ten times between September and December 2006 and in weekly intervals from February 2007 to November 2007. Additionally, hydraulic pressures were recorded continously from October 2006 to July 2007 in piezometers F1 to F4 and from July 2007 to July 2008 in piezometers F2, F4 and F5. Barometric pressure measurements at a nearby station were used to correct the hydraulic pressure readings. There was a range of additional data available from a monitoring project of the federal waterway authority *viadonau* including hourly river water levels from a gauging station at Hainburg at the downstream end of the domain and river water levels simulated by a hydrodynamic surface water model (Tritthart [30]). A lidar based digital elevation model and ground surveys conducted in 2006 were used to represent topography. The information about the subsurface was based on bore hole data of the Austrian Hydropower AG collected in 1981–82. Within the model boundary 25 bore hole profiles were located, 13 of those distributed over the southern part of the domain and the rest situated along the riverbed. The bore profiles provided top and bottom elevation of the gravelly aquifer.

2.1.1. Measurements of hydraulic parameters

In October 2007 two infiltrometer tests were carried out near piezometer F5. The estimated hydraulic conductivity for the coarse gravel layer was 0.02 m/s. The sediment properties of the riverbed

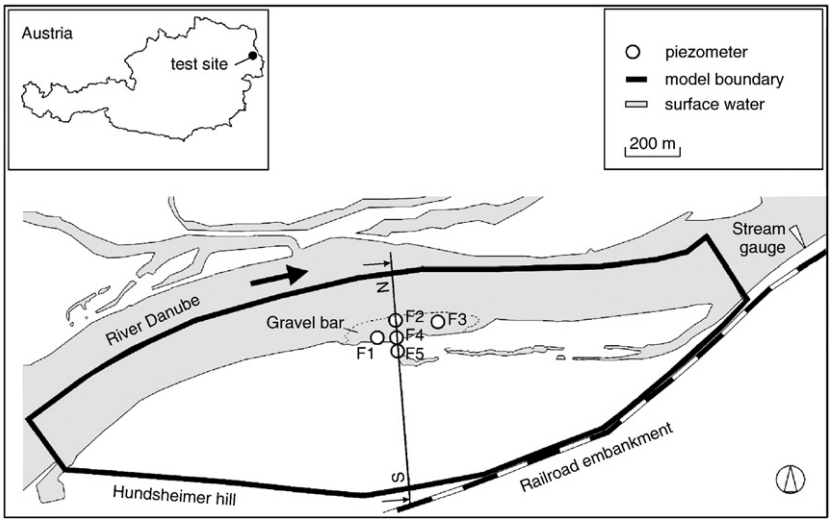

Fig. 1. Map of the field site (48° 9′ N, 16° 57′ E), observation points and model boundary; grey shading indicates surface water (Danube river and secondary channels) at mean water level. Locations of the cross section N–S (Fig. 2) and the river gauge are indicated.

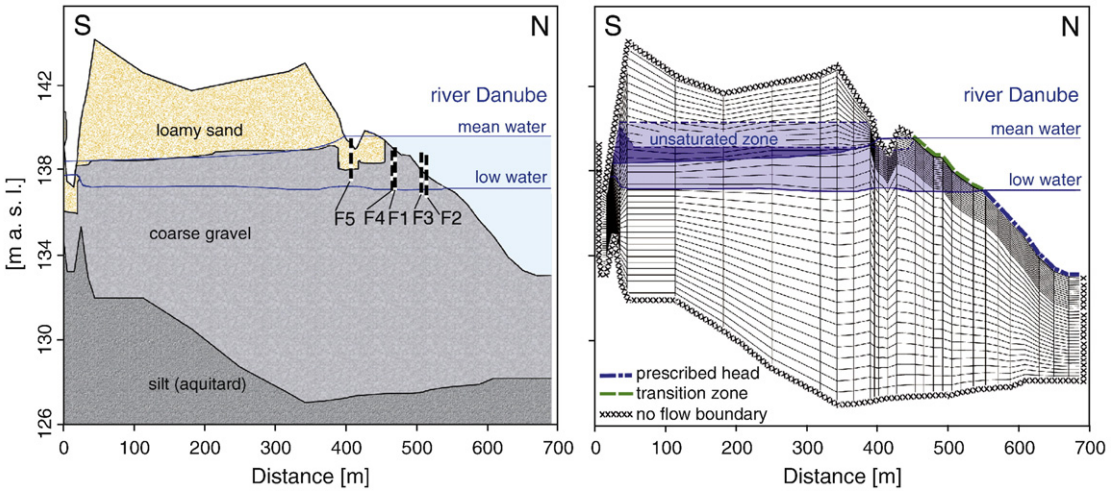

Fig. 2. Cross section N–S through the model as shown in Fig. 1. Hydrogeological layers within the model domain; Piezometer locations, mean and low water levels together with simulated groundwater levels are indicated (left). Setup of the numerical mesh for cross section N–S (right); the boundary conditions are shown: prescribed head: $h(t) = h_{river,t}$; no-flow boundary: $q = 0$; and transition zone, where either $h(t) = h_{river,t}$ if $h_{river,t} > h_{groundsurface}$ or $q = 0$ if $h_{river,t} \leq h_{groundsurface}$. The extents of the unsaturated zone for mean and low water levels are indicated in blue shading (right).

were determined by sieve analyses from undisturbed probes taken by the *Freeze panel* method (Niederreiter and Steiner [23]). The panels were analysed separately for the upper 10–15 cm layer and the layer below 15 to 30 cm. The grain size distributions of samples taken near the gravel bar are shown in Fig. 3.

2.2. Model setup

Sutra2D3D (Voss and Provost [32]) was used for simulating the three-dimensional groundwater flow patterns. The horizontal discretisations of the numerical elements vary between 5 and 100 m. Smaller cell sizes are needed near the riverbanks to ensure the convergence of the pressure solutions in the unsaturated zone. The aquifer below the riverbed was hence discretised into 37 layers ranging from 5 to 40 centimetres (Fig. 2, right). The model consisted of nearly 200,000 elements in total. The conductance of the riverbed is represented by the hydraulic conductivity, which is assumed anisotropic and heterogeneous within the model domain (Section 3). The modelled leakage from or into the aquifer hence depends on the hydraulic pressure gradients between the river and the groundwater levels and conductivities. Anisotropy and heterogeneity of conductivities result in spatial and temporal differences in the leakage characteristics. It is important to note that, for modelling the exchange fluxes across the river–aquifer interface, this approach can only be applied in conjunction with time-dependent simulations. The time step sizes were 30 min.

The model solves the general form of the three-dimensional variably saturated groundwater flow equation (Voss and Provost [32], p.26, Eq. (2.24)). The numerical solution of this equation is processed by at first linear projection of the nodal heads and iterative processing for resolving nonlinearities. Then the linear system of equations is solved using an iterative sparse matrix equation solver.

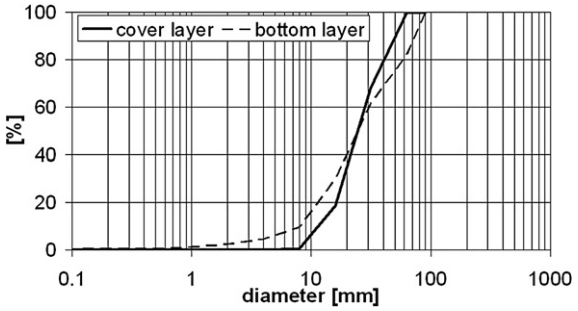

Fig. 3. Sieve curves of the cover (10–15 cm) and of the layer below (15–30 cm) from undisturbed probes of the riverbed near the gravel bar (*Freeze panel* method (Niederreiter and Steiner [23])).

Water saturation S_w and relative permeability k_r are represented by the *van Genuchten* model (van Genuchten [31]), with the parameters a, n and the residual water saturation S_{wres} (Voss and Provost [32], p.16, Eq. (2.8) and p.24, Eq. (2.21a,b)). For the gravel part of the aquifer, the parameters a, n and S_{wres} were set to 1.53 kPa^{-1}, 2 and 0.18, respectively as determined by lab experiments of the *Institute for Land and Water Management Research, Petzenkirchen*. For the fine sands, the parameters were set to 0.36 kPa^{-1}, 3.18 and 0.14, as obtained by the *Rosetta Lite* program (Schaap et al. [28]) for the sand textural class of the USDA triangle.

In order to ensure that Darcy's law is still valid within the highly permeable aquifer, we calculated the Reynold's number *Re*, given by $Re = \rho \cdot v \cdot d_{10}/\mu$ (de Marsily [10]), where d_{10} is the effective diameter of the grains, which was taken as 10 mm according to the sieve curve analysis (Fig. 3). μ is the dynamic viscosity of the fluid and ρ the fluid density. The Reynolds number never exceeds 0.7 during the calibration period. Groundwater flow is hence laminar ($Re < 2$) and Darcy's law is valid (de Marsily [10]).

We also performed transport simulations which were based on the advection–dispersion equation. *Sutra2D3D* (Voss and Provost [32], p.31, Eq. (2.31)) solves this equation simultaneously with the groundwater flow equation. The spatial discretisation for transport were set as for the groundwater flow simulations, while the time steps were reduced to 10 min.

2.2.1. Boundary conditions

The model domain's northern zone is overlain by the river Danube and is on average 200 m wide (Fig. 1). In this zone prescribed head boundary conditions were used for the top elements based on the recorded river water levels from the Hainburg gauge in 30 minute intervals and the water levels from a three-dimensional surface water model (Tritthart [30]). In this way the dynamics of river flow and their effect on groundwater flow were fully accounted for. Effects of groundwater–river exchange fluxes on river flow processes will be insignificant as they are several orders of magnitude smaller than the total river discharge. The top layer in the landzone was set to a no-flow boundary condition, since groundwater recharge was negligible during the simulation period. The transition zone between the highest and lowest water mark alternates between submerged and dry (Fig. 2,

right). The boundary conditions in this zone were set according to the model result of the previous time step for a given node. If the hydraulic pressure of the previous time step was positive, the head boundary condition was set to the local surface water level. If the hydraulic pressure was negative, the boundary conditions were set to no-flow since the soil was unsaturated. The bottom model boundary was set to a no-flow boundary because of the clayey silt aquitard below. The levels of the top of the aquitard were interpolated from bore profile information. The vertical southern boundary was set to no-flow as the gravel layer is very thin. This boundary follows the base of the *Hundsheimer* hill. The vertical northern boundary was set to no-flow assuming parallel flow along this boundary. All boundary conditions are shown in Fig. 2, right.

3. Model calibration and validation

For model calibration a nine day period in October/November 2006 was simulated. During this time, the flow situation changed twice from predominant groundwater exfiltration to infiltration conditions due to rapidly rising river water levels. This period was considered well suited for calibration because the groundwater levels were little influenced by the river boundary (low water in the river) and the river water levels were fluctuating, so that the effects of a change from groundwater exfiltration to infiltration conditions and vice versa, could be investigated. This period is therefore well suited for investigating the effects caused by transient river water levels on the flow patterns in the surface water–groundwater mixing zone. The calibration procedure consisted of the following steps: At first a homogeneous distribution of the hydraulic conductivity and porosity for the gravel aquifer was assumed with values of 0.001 m/s and 0.15 throughout the model domain. This first assumption resulted in root mean square errors (RSME) of 8–12 cm and showed that the porosity had to be decreased in order to reduce the attenuation of the simulated groundwater levels. Then the hydraulic conductivities within the calibration zone were increased by a step-wise approach starting around piezometer F1 (Fig. 1). After the simulated groundwater levels matched the observations for piezometer F1, the hydraulic conductivity between piezometers F1 and F2 was increased until results at F2 agreed well with the observations. The procedure was repeated for piezometers F4 and F3, in this order, according to their alignment along the main groundwater flow direction. The RSME were reduced to 3–4 cm, with hydraulic conductivities in the gravel aquifer set to 0.002–0.03 m/s and porosities set to 0.09. The calibration simulations suggested that groundwater levels were most sensitive to hydaulic conductivity and porosity. The aquifer depths were not changed because they were based on bore profile information. The hydraulic conductivity of the fine sand layer was set to $9 \cdot 10^{-5}$ m/s, as obtained by the *Rosetta Lite* program (Schaap et al. [28]) and the porosity was set to 0.2 (McWhorter and Sunada [21]). Based on existing knowledge on the general geologic structure of fluvial deposits hydraulic conductivity was assumed to be anisotropic. A layered structure is typical for this type of sedimentary environment. Due to permanent lateral movements of the river bed to the temporary deepest location of the plain, large lowlands were formed over geologic time periods (Promny [25]). Also at our study site, layering can be expected. Accordingly, the hydraulic conductivities in vertical direction were set to 10% of those in horizontal direction, as also reported in the literature (Chen [9]). The parameters describing the unsaturated zone were kept constant because they did not affect the simulated groundwater levels significantly.

The best estimates for the hydraulic conductivities agree well with infiltrometer tests near the calibration region ($K = 0.02$ m/s, Section 2.1.1). The transient simulations reproduced the dynamic hydrographs of the continously observed groundwater levels in piezometers F1 to F4 well (Fig. 4). The river water levels set as boundary at cross section CD are additionally shown for comparison. The differences between river and groundwater levels change in time due to the effect of river–aquifer interactions.

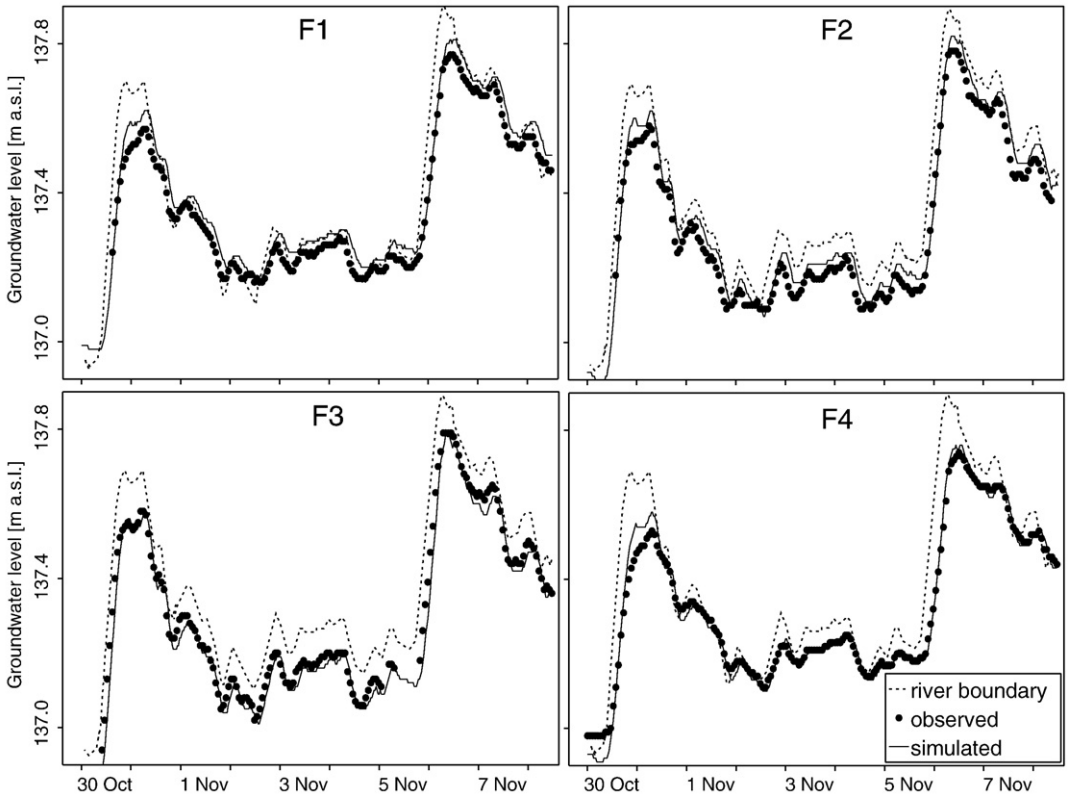

Fig. 4. Groundwater hydrographs during a 9 day low groundwater period at observation points F1, F2, F3 and F4 (see Fig. 1); dashed lines indicate the river water levels set as specified head boundary at cross section CD (Fig. 8); calibration period: 30 Oct to 8 Nov, 2006.

The model was validated for two separate time periods. The first is a 13 day period in February 2007, during which the river water level first rose to 80 cm above the ground surface of the gravel bar and then dropped to 40 cm below the ground surface. This is a useful validation period as the groundwater levels in the gravel bar are by 1 m higher than during the calibration period and the ground surface alternates between wet and dry conditions. The second time period was chosen in November/December 2007 during which the groundwater levels fluctuated more strongly than during the other simulation periods and where the simulations were checked against piezometer F5 not used in the calibration. This observation point is located 60 m from the calibrated zone (Fig. 1). For both validation periods the simulated water levels agree very well with the observed water levels (Fig. 5). The mean differences are always less than 7 cm.

4. Results

4.1. Groundwater gradients and exchange fluxes

The groundwater gradients were estimated by subtracting the observed groundwater levels in piezometer F4 from F2. In this way, their lateral components were investigated in perpendicular direction to the river bank. Fig. 6 shows that the lateral gradients are positive most of the time, meaning that they are inclined towards the centre of the river axis. This means that the predominant situation is groundwater exfiltration into the Danube river. Only during rapidly rising river water levels the flow direction reverses for a couple of hours up to two days at maximum. River water fluctuations greater than 1 m are a result of precipitation events or snow melt in spring. Smaller river water fluctuations are due to upstream control measures at hydropower plants. The time-lag between groundwater level fluctuations that are close to the river (piezometer F2) and those that are 40 m away (piezometer F4) were 1.5 h on average (Fig. 4). This translates into a propagation celerity of 640 m/d, which is here defined as the speed of the groundwater wave propagation from the river, and was calculated by dividing the distance between the piezometers by the time-lag between the groundwater level peaks.

4.1.1. Dynamic storage effects on exchange flow rates

Both the infiltration and exfiltration flow rates [l/s] across the riverbed were calculated for a three day period (Nov 4–6, 2006) during an exfiltration–infiltration cycle as the sum over the submerged zone shown in Fig. 8. The transient simulations show that for both groundwater exfiltration and infiltration the exchange rates vary strongly with time in correspondence with the lateral water level gradients in the aquifer close-by the river (Fig. 6). The infiltration rates vary between 6 and 82 l/s within the detailed section (Fig. 8) and peak on Nov 6, 2006 after rapidly rising river levels. The groundwater exfiltration rates vary between −5 and −35 l/s in the detailed section. The smallest exfiltration rates occur locally during the 9 hour period with predominating infiltration.

4.1.2. Scenarios of riverbed clogging

The physical process of clogging is often of concern at locations with low river flow velocities. It can significantly alter the groundwater flow velocities in the near-stream aquifer and can therefore have adverse effects on macrozoobenthos or fish eggs.

To gain additional insight into the river–aquifer interactions, the effect of a 15 cm clogged layer on the exchange flow rates and on the groundwater hydrographs near the river was hence examined. For simulating clogging processes the same model was used as described in Section 2.2 with the difference that the riverbed was discretised

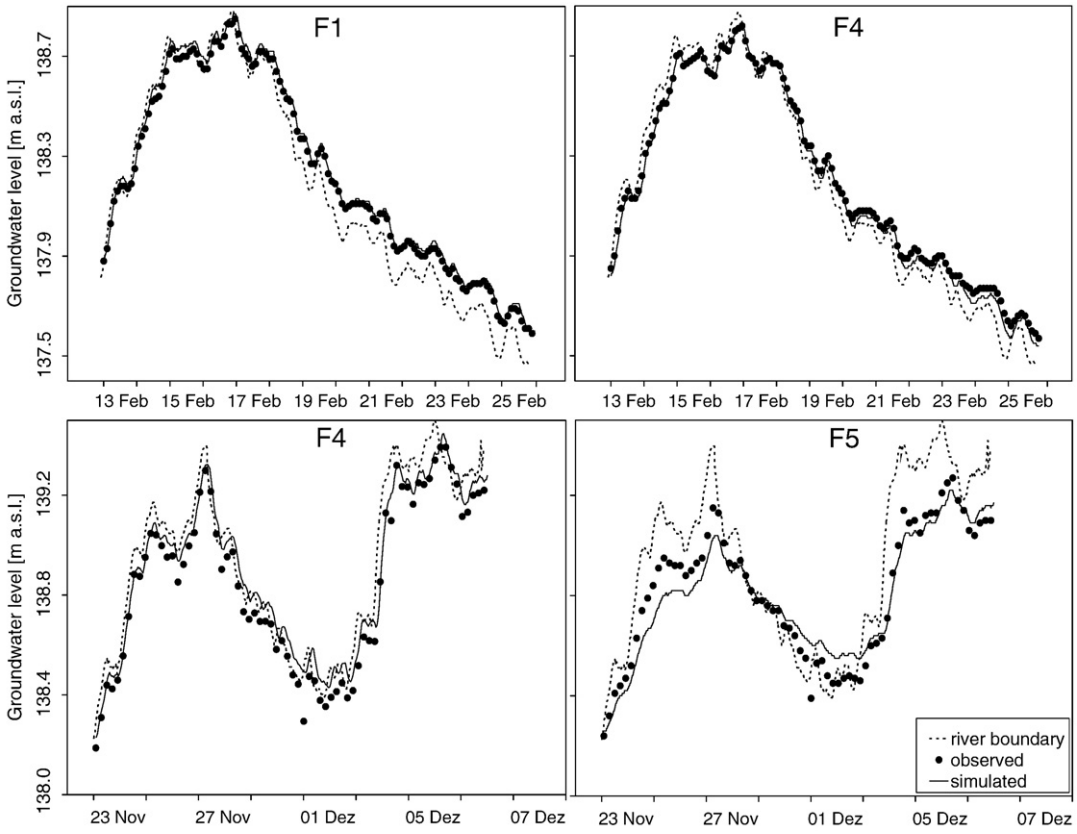

Fig. 5. Groundwater hydrographs during 14 days in February 2007 of low to mean water levels (top) and during 15 days in November/December 2007 of mean water level in the river Danube (bottom); dashed lines indicate the river water levels set as specified head boundary at cross section CD (Fig. 8); validation periods. Piezometer F5 was not used for calibration, so it provides extra information on the spatial consistency of the model.

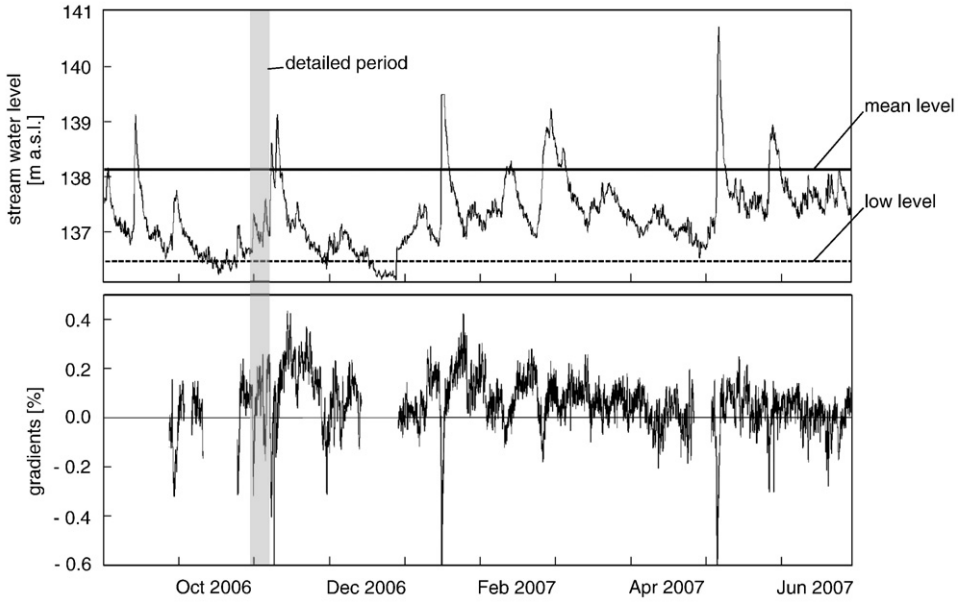

Fig. 6. Observed water levels at Hainburg river gauge (top); lateral water level gradients in the aquifer close-by the river estimated by subtracting the continuously observed groundwater levels in piezometers F2 and F4 (+groundwater exfiltration, −infiltration) (bottom). September 2006–June 2007. Detailed period relates to Figs. 4, 7–10.

using a refined vertical cell size of 2 cm. This way, the correct simulation of a thin layer of very low conductivity on the uppermost elements of the riverbed was ensured. This layer was assumed to have a thickness of 15 cm and a hydraulic conductivity of 10^{-7} m/s, which was considered as practically impermeable. The porosity was set to 9%. Two worst-case scenarios were examined, (a) a scenario where the entire riverbank was assumed to be clogged, and (b) a scenario where the entire riverbed and the river bank were assumed to be clogged. The results of the two scenarios are shown in Fig. 7. The groundwater level amplitudes are somewhat attenuated for scenario a) and clearly attenuated for scenario b).

The infiltration and groundwater exfiltration rates over the detailed monitoring zone (Fig. 8) were again evaluated. These results (not shown) indicate that the groundwater exfiltration rates are reduced to 19–77% after clogging of the banks and to 0–5% after clogging of both the riverbed and bank sides compared to the original rates. The infiltration rates are reduced to 0–55% after clogging of the banks and to 0–5% after clogging of both the riverbed and bank sides.

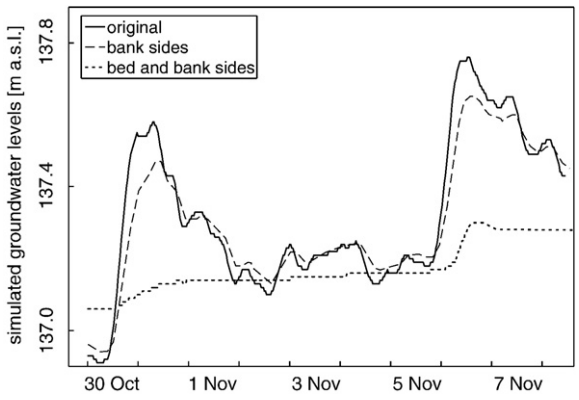

Fig. 7. Groundwater levels simulated at observation point F4 (see Figs. 1 and 4) during Oct 30–Nov 8, 2006. Original hydraulic soil properties (continuous line), after clogging of the top 15 cm layer of the river bank (dashed line) and after clogging of the top 15 cm layer of both the riverbed and the bank (dotted line).

4.2. Three-dimensional flow patterns

In this section the simulation results of the three-dimensional groundwater flow patterns in the gravel bar are presented for a three day period (Nov 4–6, 2006) during an exfiltration–infiltration cycle. The lateral water level gradients (between piezometers F4 and F2, estimated as described in Section 4.1) in the aquifer close-by the river are 0.19% (predominant gw exfiltration) at the beginning of the period and then decrease to −0.27% (predominant gw infiltration). Due to the dampening of the groundwater response, the maximum lateral gradients occur 10 h before the absolute river water level peak. This is when the river water levels increase the most rapidly, which results in high lateral groundwater gradients in the aquifer close-by the river. The history of river water fluctuations is hence a key factor for judging the actual flow situation. In Fig. 8 the flow directions and contours of the absolute velocity magnitudes in the bottom model layer are shown in map view. All velocities shown there are pore-water velocities, whereas the river indicated in light blue is above the aquifer. Fig. 8, top left shows the groundwater flow directions after a quasi-steady-state simulation. By quasi-steady-state simulation we mean that all boundary conditions are held constant over a time long enough that the initial conditions have no influence on the groundwater flow results. The steady-state simulation was solved explicitly for a simulation time of 1.5 years. Fig. 8, top right and bottom show the groundwater flow directions after transient simulations at three times starting from predominant gw exfiltration (top right), turning gw flow directions (bottom left) to predominant gw infiltration (bottom right). In Fig. 9 the flow patterns of three cross sections are shown (AB, CD and EF, as indicated in Fig. 8, top left), and in Fig. 10 those of the transect GH. The colours indicate the pore-water velocity magnitudes within a cross section or transect, respectively.

Perpendicular to the river axis (Fig. 9, top), the groundwater flow directions are predominantly parallel to the horizontal plane based on the steady-state simulation. Fig. 9, second from top, centre and right shows that circular flow patterns occur during predominant gw exfiltration. These developed during the transient simulation due to variations in river water levels. During beginning surface water infiltration the flow directions changed (Fig. 9, third from top) and the flow velocities increase with increasing lateral groundwater gradients (Fig. 9, bottom). The flow directions show again circular flow patterns.

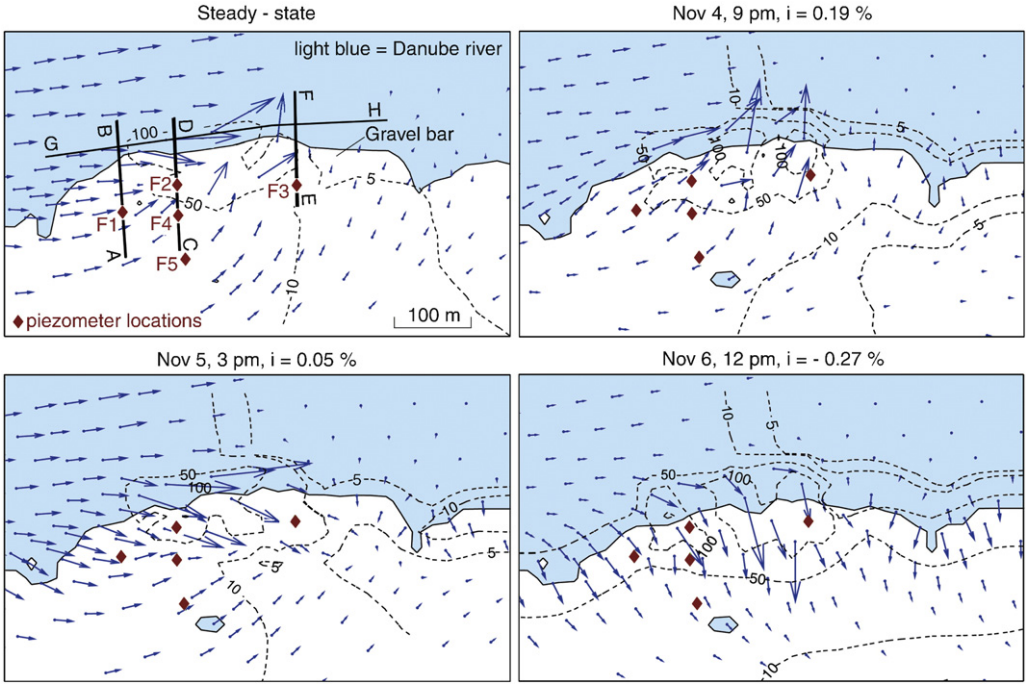

Fig. 8. Map view of horizontal groundwater flow directions (arrows) and contours of pore-water velocity magnitudes for the bottom model layer (dashed lines [10^{-6} m/s]); from top: quasi-steady-state simulation and 3 transient simulation times during a three day period (Nov 4–6, 2006) and an exfiltration–infiltration cycle with decreasing lateral gradients, *i*, in the aquifer close-by the river (+groundwater exfiltration, −infiltration, estimated as described in Section 4.1); River zone is indicated by light blue shading. In the top left figure the cross and longitudinal sections are indicated (see Figs. 9 and 10).

Fig. 9, left side, top to bottom shows that groundwater flow directions are downwelling on the upstream end of the gravel bar near piezometer F1.

Parallel to the river axis these downwelling patterns are evident at the upstream end of the gravel bar even during periods with predominant groundwater exfiltration (Fig. 10, first three from top). During these periods, upwelling flow is present at the downstream end of the riffle, where groundwater is discharged into the river. Downwelling flow occurs both at the upstream and the downstream end of the gravel bar during predominant infiltration (Fig. 10, bottom).

In contrast to the transient simulations, the quasi-steady-state simulations do not show any circulation of groundwater flow (Fig. 9, top). This means that the time history of the river hydrograph generates distinct flow patterns in the surface water–groundwater mixing zone, which will affect the transport pathways of substances in the subsurface. The magnitude of flow velocities strongly depends on the lateral water level gradients in the aquifer close-by the river.

4.2.1. Transport simulations of conservative tracer

In order to understand solute transport processes at the study site, the pathways of a conservative tracer distributed homogeneously in the river were simulated. The dispersivity values for the horizontal directions were taken from the results of tracer tests conducted in the Seewinkel nearby lake Neusiedl where the soil properties are similar to the field site at the Danube (Gutknecht et al. [15]). The longitudinal and transversal dispersivities for the horizontal direction were set to $\alpha_{L,hor} = 7\ m$ and $\alpha_{T,hor} = 2$ m, respectively. The ratio between vertical to horizontal dispersivities was set in consistency with the sedimentary origin of the aquifer, with $\alpha_{L,vert} = 0.7\ m$ and $\alpha_{T,vert} = 0.35$ m. This is consistent with a ratio $\alpha_{L,T,vert}/\alpha_{L,T,hor}$ of approximately 0.1 as reported in the literature (e.g. Gelhar et al. [14], Garabedian et al. [13]). In order to keep the numerical dispersion smaller than the physical dispersion, sufficiently small temporal and spatial discretisation are needed. For small ratios of α_L/α_T (<10), as in our simulations, and for the three-dimensional case, the following conditions should be fulfilled (Kinzelbach [18]): $P_e = v \cdot \Delta d/D \leq 2$, where P_e is the *Peclet* number, D is the dispersion coefficient, Δd is the maximum element size and v is the pore-water velocity. In our case, this condition is fulfilled over the whole detailed section (Fig. 8), with maximum P_e of 2 in horizontal and 0.6 in vertical directions. The second condition concerns the time steps (Δt) and is the *Courant* criterion, Co: $\Delta t \cdot v/\Delta d \leq 1$. With a time step of 30 min in the simulations, Co never exceeds 0.27, which satisfies the criterion.

The initial concentrations were set to 50 mg/l throughout the whole model domain. As a boundary condition a constant tracer concentration of 100 mg/l was set over the entire river area of the model. The boundary conditions for simulating gw flow were set as described in Section 2.2.1.

A simulation period different from that of the calibration was chosen (Oct 5–24, 2006). The period starts with two days of predominant infiltration into the aquifer followed by 17 days of reversed flow conditions. At the beginning of the period the gravel bar was half a metre above the water and then was slowly submerged with water depths of 20–50 cm. These model simulations allow another validation of the model. The maximum differences between simulated and observed groundwater levels at the observation wells F1, F2, F3 and F4 (Fig. 1) are 7 cm (not shown).

The simulated solute breakthrough curves at the observation points F1–F3 (see Fig. 1) are shown in Fig. 11. During the first 2 days of simulation, the conservative tracer is transported into the aquifer due to higher surface water levels and hence enhanced infiltration of the solutes into the subsurface. According to the simulation results, the concentration curves peak after two days of predominant infiltration and then slowly decrease to a slightly augmented concentration value. These somewhat higher concentrations compared to the background concentration suggest that even if most of the groundwater is discharged into the river, small amounts of surface water will pass through the gravel bar. The distinct tails of the breakthrough curves (Fig. 11) are related to low lateral groundwater gradients during predominant groundwater exfiltration into the river, so little exchange. Also some

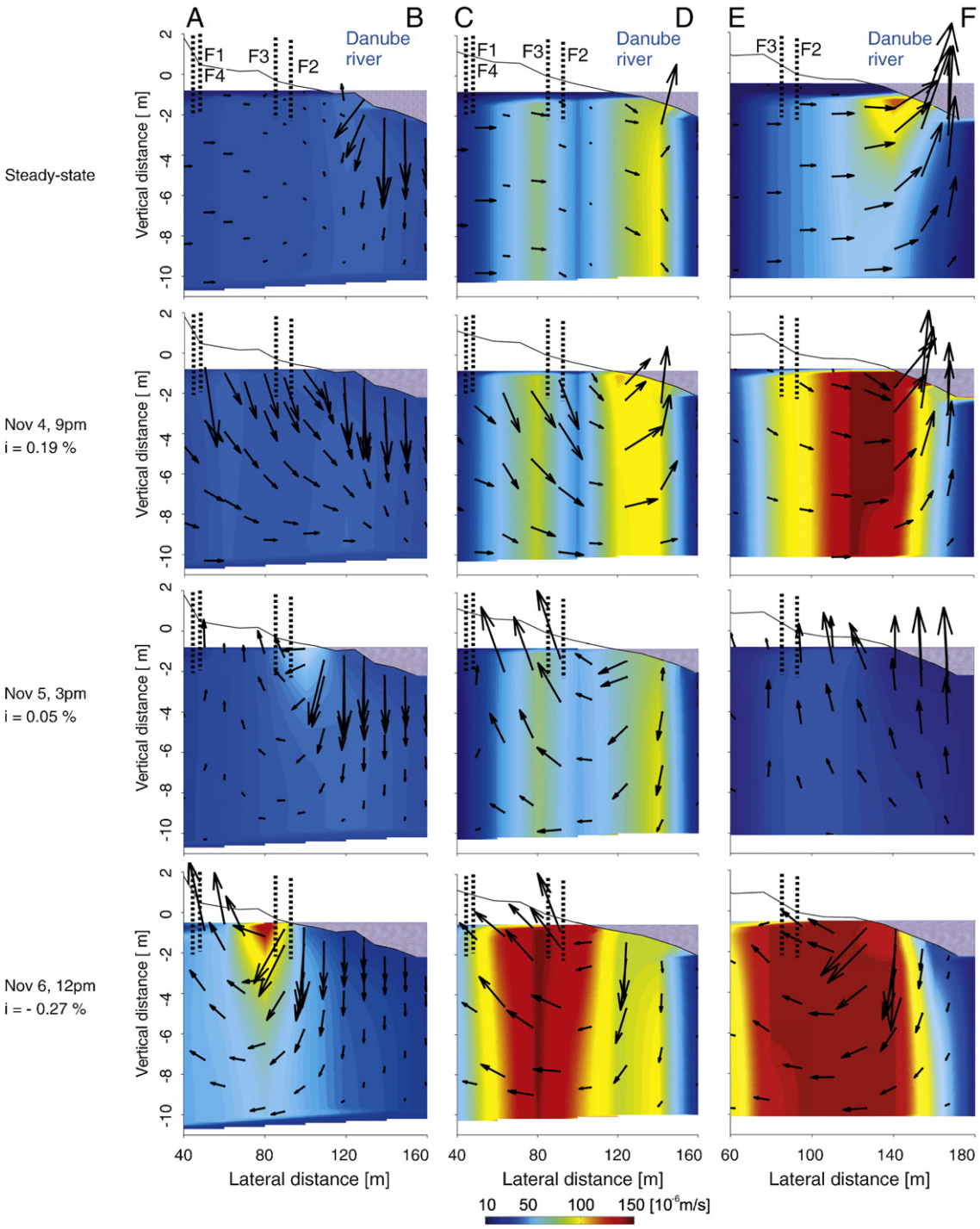

Fig. 9. Cross sections (AB, CD and EF, see Fig. 8) of groundwater flow directions (arrows) and pore-water velocities (colours); from top: quasi-steady-state simulation and 3 transient simulation times during a three day period (Nov 4–6, 2006) and an exfiltration–infiltration cycle with decreasing lateral groundwater gradients, *i*, in the aquifer close-by the river (+groundwater exfiltration, −infiltration, estimated as described in Section 4.1); River zones are indicated by blue shading. solid black line: ground surface; white area indicates unsaturated zone.

infiltration and mixing persist at the gravel bar even during predominant groundwater exfiltration. At observation point F4 no significant increase of concentrations is observed, so they are not shown here.

As mentioned before, the concentration peaked in the aquifer after two days of simulation time due to permanent predominant infiltration. This point in time was used as a starting point for two different simulations in order to investigate the significance of river water fluctuations on the dilution of solutes in the aquifer close-by the river: Both simulations were initialised with the simulated concentrations at this point in time and were run for 17 days. The first simulation was continued with the transient groundwater flow patterns. The observed river levels were used as a boundary condition. The second simulation was initialised with steady-state groundwater flow patterns, which were simulated with a constant river level boundary observed at the initial time as described in Section 4.2. The river levels were held constant over the 17 days of simulation time. As compared to the transient simulation, the concentrations are much higher towards the end of the period (at observation points F1, F2, Fig. 11).

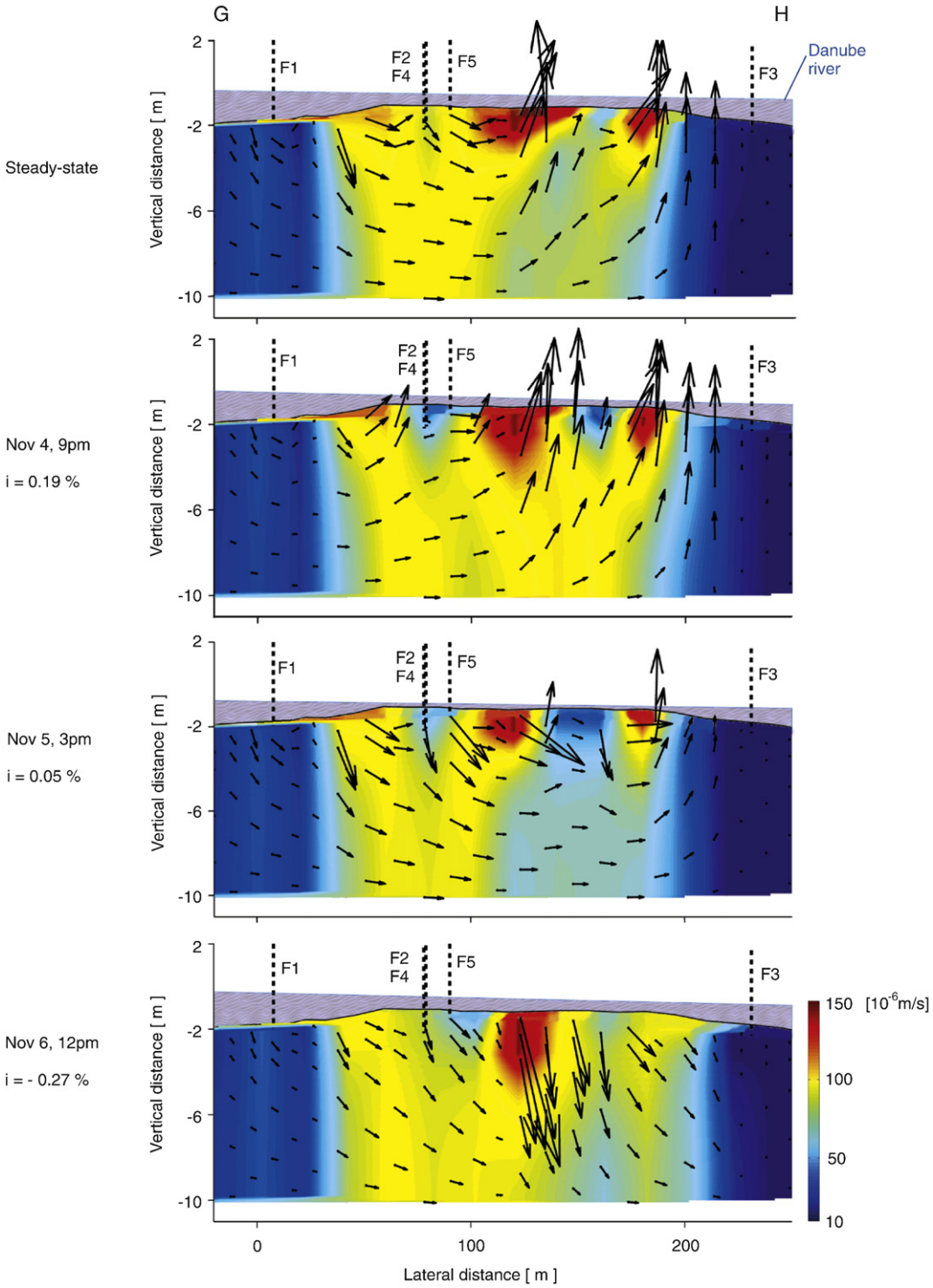

Fig. 10. Transect through the gravel bar (GH, see Fig. 8) with groundwater flow directions (arrows) and pore-water velocities (colours) shown; from top: quasi-steady-state simulation and 3 transient simulation times during an exfiltration–infiltration cycle with decreasing lateral groundwater gradients, *i*, in the aquifer close-by the river (+groundwater exfiltration,−infiltration, estimated as described in Section 4.1); river zones are indicated by blue shading. Solid black line: ground surface.

In order to investigate why the concentrations in the transient case are lower than in the quasi-steady-state case, the groundwater flow directions (Fig. 12, arrows) and the concentration distributions of the conservative tracer (Fig. 12, colours) are shown in detail for three cross sections (A–B, C–D and E–F). The top row shows the results after two days of predominant infiltration. During this time circular flow patterns were formed, which developed due to the variation of river water levels over time. These patterns lead to an enhanced mixing between surface water and the aquifer and apparently widen the extent of the surface water–groundwater mixing zone from looking at Fig. 12, top. Two different simulations are compared in the centre and bottom rows, which both show the concentration distributions after a 17 day simulation period that was initialised with conditions on day 2. The results in the centre row refer to the quasi-steady-state simulation in

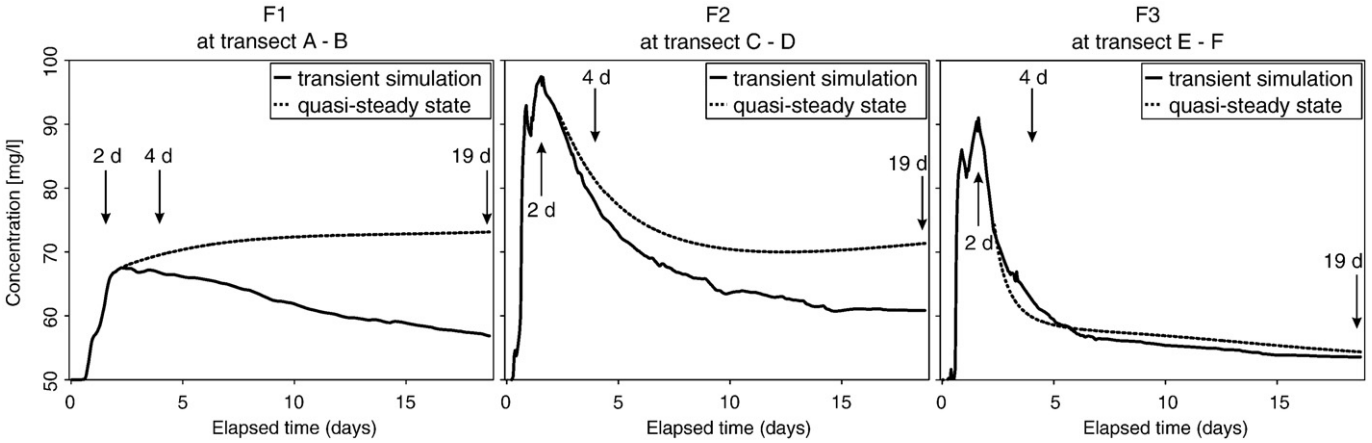

Fig. 11. Simulated concentration breakthrough curves at observation points F1, F2 and F3 (Fig. 1) for a conservative tracer simulated with constant $c_{river} = 100$ mg/l river boundary conditions. For comparison a case with a quasi-steady-state gw flow field. Both simulations are identical for the first 2 days of simulation time during which groundwater infiltrated due to rising river water levels. Then both simulations were continued for 17 days of simulation time during which groundwater exfiltrated into the river and lateral water level gradients declined. The transient simulation was continued with observed river levels as boundary condition. The quasi-steady-state simulation was initialised with a steady-state flow field (as described in Section 4.2) and run with a constant river boundary. Time 0 is Oct 5, 2006. Times chosen for showing the tracer distribution: in transects AB, CD and EF (Fig. 12) are indicated by arrows.

Fig. 11 and results in the bottom row refer to the transient simulation. During both simulations, predominant groundwater exfiltration led to a lateral movement of the concentration plume towards the centre of the river. This is demonstrated by comparing the location of the red zones in Fig. 12, top with the centre and bottom rows. In order to investigate, why the concentrations in the mixing zone are reduced faster in the time-dependent simulation than in the quasi-steady-state simulation (Fig. 11), the groundwater flow directions were compared. Fig. 12, centre and bottom rows (arrows) show the groundwater flow directions two days after initialising the simulations because then distinctly different flow fields between steady-state and transient simulation occur. According to the quasi-steady-state simulation, the groundwater flow directions are mainly parallel to the horizontal plane and are upwelling below the riverbed. The river water level variations, however, induce transient storage phenomena, which lead to complex groundwater flow patterns in the river–aquifer mixing zone. This explains why the conservative tracer concentrations are reduced faster at observation points F1, F2 and F3, namely because they are more strongly diluted within the mixing zone (Fig. 11).

Flow parallel to the river axis exhibits complex patterns, too. Lower flow velocities at the downstream end of the gravel bar (Fig. 12, right column) are caused by both lower riverbed permeabilities and lateral water level gradients. As a consequence, the tracer concentrations are lower in this region.

In order to investigate the size increase of the mixing zone in a more quantitative way, the volume extents of the mixing zone from our simulation results were determined by calculating the volumes exceeding various concentration thresholds (55, 60, 70, 80, 90 mg/l) for every 30 min of simulation time. The results were compared to transport simulations, where the river water levels were held constant (Fig. 13, left). After 10 days of simulation time, the calculated volume of the 70 mg/l concentration threshold was $0.8 \cdot 10^6$ m^3 in the case of constant river water levels, as compared to $2.3 \cdot 10^6$ m^3 for the transient case (Fig. 13, right). This means that the river water fluctuations increase the size of the mixing zone by a factor of 3. In order to examine the sensitivity of the dispersivities on the calculated volumes, we performed two additional transient transport simulations, one where $\alpha_{L,H}$, $\alpha_{T,H}$, $\alpha_{L,V}$ and $\alpha_{T,V}$ were set to 5 m, 1.5 m, 0.5 m and 0.25 m, respectively, and another where these values were set to 10 m, 3 m, 1 m and 0.5 m, respectively. After 10 days of simulation time, the calculated volumes for the 70 mg/l concentration were $2.0 \cdot 10^6$ m^3 for the smaller dispersivities as compared to $2.6 \cdot 10^6$ m^3 for the larger dispersivities. This means that the effect of the river water fluctuations on the size of the mixing zone is much larger than the effect of changing the dispersivities within reasonable ranges.

5. Discussion

The study described in this paper aims to provide insights into several scientific questions that are discussed below.

In a first step, we have examined the mechanisms affecting groundwater response to river level fluctuations. The time-lag between groundwater level fluctuations that are at the river bank (piezometer F2) and those that are 40 m away from the bank (piezometer F4) are 1.5 h on average (Section 4.1, Fig. 4). This translates into a propagation celerity of 640 m/d, while the simulated pore-water velocities between F2 and F4 range between 1 m/d and 13 m/d (Fig. 9). Obviously, propagation celerities are much faster than flow velocities. Lewandowski and Nützmann [19] observed a 2 h time-lag between peaks of the River Spree and the groundwater level in a piezometer at 25.5 m distance (propagation celerity = 306 m/d), and calculated an average velocity of 0.43 m/d based on measured K-values, lateral water level gradients and porosity. They referred to a statement of Brown et al. [6] that the celerity of pressure changes is usually more than 100 times faster than the flow velocity.

The river–aquifer exchange seems to be strongly influenced by transient storage phenomena (Fig. 6). Predominant groundwater exfiltration was reversed during rapidly rising river water levels leading to predominant infiltration at the river banks. This is a phenomenon also observed by Lewandowski and Nützmann [19], who measured the lateral gradients between the River Spree and the groundwater levels 25.5 m from the river. The observed gradients ranged between $\pm 0.6\%$ and are of the same order of magnitude as those in this paper (Fig. 6).

Simulations of clogging scenarios of the riverbed showed significant attenuation of the groundwater fluctuations near the river, which is what one would expect. This is consistent with a study that was performed 30 km upstream of the study site in the impoundment of a hydropower plant (Gutknecht et al. [16], Blaschke et al. [2]). Based on undisturbed sediment samples of the riverbed (Niederreiter and Steiner [23]), they found clogging layer depths of 5–20 cm, while, in this paper, a depth of 15 cm was assumed. Blaschke et al. [2] also found significant spatial and temporal variability of the clogging processes by using video techniques. This will have additional effects on the groundwater response. In this paper, worst-case scenarios were investigated, by simulating complete clogging of either the river bed or both riverbed and bank sides.

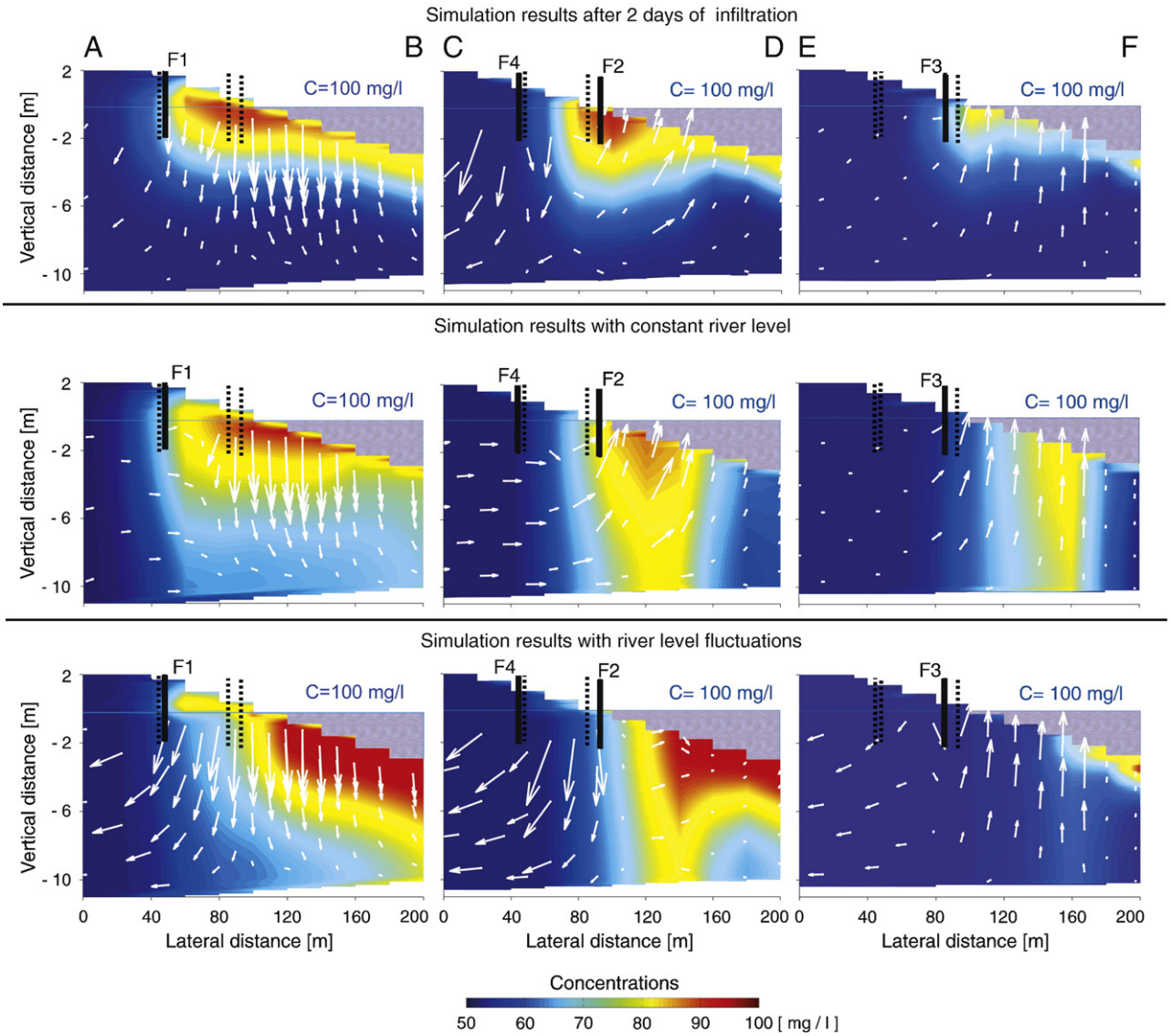

Fig. 12. Cross sections (AB, CD and EF, see Fig. 8) of simulated conservative tracer concentrations (colours) and groundwater flow directions (arrows) with constant $c_{river} = 100$ mg/l river boundary conditions; Top: transient simulation results after two days of continuous predominant infiltration and beginning predominant groundwater exfiltration; centre and bottom: for comparison between steady-state (centre) and transient simulations (bottom) the concentration distributions (colours) after 17 days of simulation time are shown during which groundwater exfiltrated into the river; The gw flow directions (arrows) after 2 days are shown because they affect later tracer transport; centre: the quasi-steady-state simulation was initialised with a steady-state flow field (as described in Section 4.2) and run with a constant river boundary. Bottom: The transient simulation was continued with observed river levels as boundary condition. Blue shading top right of each panel indicates the Danube.

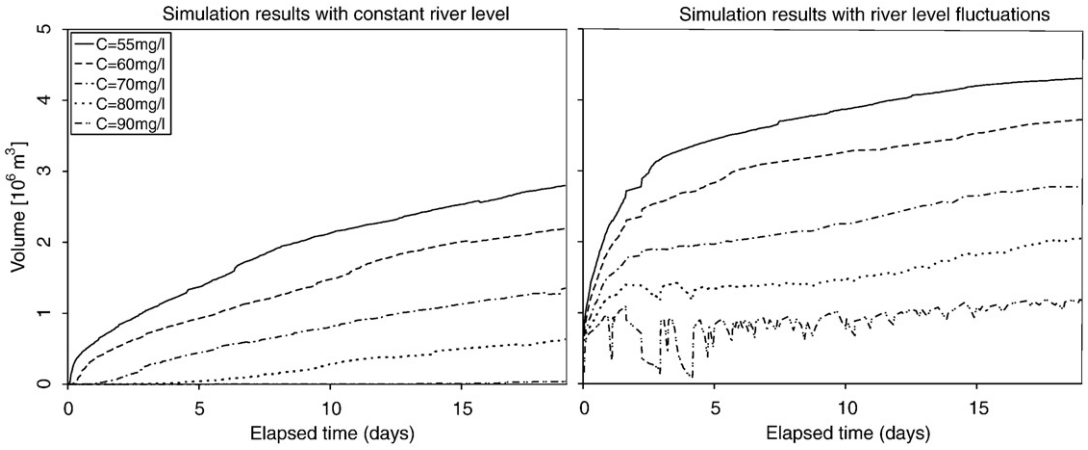

Fig. 13. Volumes exceeding various threshold concentrations (55, 60, 70, 80, 90 mg/l), estimated from the simulations in Figs. 11 and 12. Left: simulation results with river water levels held constant; right: simulation results with river water levels changing in time. Time 0 is Oct 5, 2006.

In a second step, we examined the effect of short-term (6–48 h) river level fluctuations on the size of the river–aquifer mixing zone and on enhanced dilution of the solute concentrations. Groundwater flow and transport simulations showed circular flow patterns near the surface water–aquifer interface induced by the dynamics of the river water levels (Fig. 9). These patterns produced an extended surface water–aquifer mixing zone (Fig. 13) and enhanced the dilution of solute concentrations (Fig. 11).

Tidal fluctuations have a similar effect as river water fluctuations and induce circular flow patterns at the seawater-aquifer mixing zone as shown by Robinson et al. [27]. The tidal range at their study site of 1–2 m was similar to the amplitudes observed at the river Danube (Fig. 6). While tidal fluctuations are regular with a time scale of 12 h, the time scales of river water fluctuations at the field site presented here varied between 12 h and a few days. Therefore, it was important to understand if enhanced mixing only occurs with a certain number of fluctuation cycles. While at the seawater site of Robinson et al. [27] tidal induced mixing was investigated after multiple tidal cycles, the enhanced mixing effects at the Danube site were investigated after one infiltration–exfiltration cycle.

A similar study by Lu et al. [20] in a coastal aquifer found that the width of the mixing zone was positively correlated to the dispersivities, which is consistent with our sensitivity analysis (Section 4.2.1). However, in our study the size increase of the mixing zone is mainly due to the variation of the groundwater flow field, as shown by the development of circular flow patterns (Fig. 9), and to a lesser extent to dispersion effects. In this study, the effects of small-scale heterogeneities were lumped into the dispersion parameters. Fleckenstein et al. [12] suggest that small-scale heterogeneities may cause strong variations in the spatial patterns of seepage along the river channel, water level and connectivity. An alternative to lumping the small-scale heterogeneities into dispersivity would be to perform random walk simulations (e.g. Berkowitz et al. [1]).

Finally, we examined to what extent river water fluctuations increase the exchange rates between surface water and groundwater. For the case of constant flux boundary conditions in the aquifer, the groundwater levels at the river–aquifer interface will also increase if the river water level is increased leading to no change in the exchange fluxes (Storey et al. [29]). However, if dynamic effects are considered, changes in the river water levels can be very important for the exchange fluxes. Short-term variations (6–48 h) in river water levels significantly increased the exchange fluxes across the river–aquifer interface in our study, which will probably also hold true for other K_v/K_h ratios than the ones used here. As described in Section 4.1.1 the highest groundwater infiltration rates (82 l/s within the detailed section of Fig. 8) occurred after rapidly rising river levels. Boutt and Fleming [5] found similar changes between exfiltration and infiltration induced by daily fluctuations in river levels associated with anthropogenic water releases from a hydropower plant at the Deerfield river in Massachusetts. Their transport simulations indicated higher mass transport of a conservative tracer into the aquifer and enhanced mixing if river levels were oscillating than if river levels were set constant. The mixing still occurred even when net exchange over a number of days was zero. At the site discussed in this paper, groundwater exfiltration prevailed. Similar to the Deerfield site, mass transport of the conservative tracer was enhanced by the changes in the flow directions.

6. Conclusions

This study found that river water fluctuations are one significant mechanism responsible for increasing the extent of the river–aquifer mixing zone. River water fluctuations therefore need to be taken into account when investigating mixing zone processes. The results also suggest that the increase of the mixing zone extent is not only caused by dispersion but also by advection, as evidenced by the circular groundwater flow patterns in the aquifer close-by the river. As solute concentrations were shown to be more strongly diluted when river water levels fluctuated than when they were constant, nutrient transport will be significantly affected. Furthermore, we found that the river water fluctuation caused variations in the groundwater velocity magnitudes within the mixing zone, which can have adverse effects on macrozoobenthos or fish eggs.

All of these findings have important implications for the management of rivers, such as the regulation of river power plants, the supply of drinking water from riverbank filtration and river restoration projects. In future work, additional tracer measurements using, e.g., multilevel samplers would be needed, in order to determine the extent of the mixing zone and the degree of solute dilution within this zone. In such a study, the challenge will be to find suitable tracers that non-ambiguously identify the influence of surface water in the aquifer. Furthermore, measurements of nutrients or microbial tracers in the river–aquifer mixing zone during transient flow conditions could provide additional insights into the effects of river water fluctuations on transport processes.

Acknowledgments

We would like to thank Christine Gschöpf and Peter Haas for their help with the field tests and surveys, Friedrich Schiemer for initiating this project and the Federal Waterway Authority *viadonau-Österreichische Wasserstraßen-Gesellschaft mbH* for financial support. We would also like to thank the Austrian Science Funds FWF for financial support as part of the Doctoral program DK-plus W1219-N22 on Water Resource Systems.

References

[1] Berkowitz B, Klafter J, Metzler R, Scher H. Physical pictures of transport in heterogeneous media: advection–dispersion, random-walk, and fractional derivative formulations. Water Resour Res 2002;38(10):1–12.
[2] Blaschke A, Steiner K-H, Schmalfuss R, Gutknecht D, Sengschmitt D. Clogging processes in hyporheic interstices of an impounded river, the Danube at Vienna, Austria. Int Rev Hydrobiol 2003;88(3–4):397–413.
[3] Boano F, Demaria A, Revelli R, Ridolfi L. Biogeochemical zonation due to intrameander hyporheic flow. Water Resour Res 2010;46.
[4] Boulton A. Stream ecology and surface-hyporheic hydrologic exchange: implications, techniques and limitations. Aust J Mar Freshw Res 1993;44:553–64.
[5] Boutt D, Fleming B. Implications of anthropogenic river stage fluctuations on mass transport in a valley fill aquifer. Water Resour Res 2009;45:1–14.
[6] Brown RH, Konoplyantesev AA, Ineson J, Kovalevsky VS. Ground-water studies. Studies a. Reports in Hydrology 7. Paris, France: UNESCO; 1975.
[7] Cardenas M. The effect of river bend morphology on flow and timescales of surface water–groundwater exchange across pointbars. J Hydrol 2008;362:134–41.
[8] Cardenas M, Wilson J. Impact of heterogeneity, bed forms, and stream curvature on subchannel hyporheic exchange. Water Resour Res 2004;40:1–13.
[9] Chen X. Measurement of streambed hydraulic conductivity and its anisotropy. Environ Geol 2000;39.
[10] de Marsily G. Quantitative hydrogeology. New York: Academic Press; 1986.
[11] Elliott A, Brooks N. Transfer of nonsorbing solutes to a streambed with bed forms: theory. Water Resour Res 1997;33(1):123–36.
[12] Fleckenstein J, Niswonger R, Fogg G. River–aquifer interactions, geologic heterogeneity, and low-flow management. Ground Water 2006;44:837–52.
[13] Garabedian SP, LeBlanc DR, Gelhar LW, Celia MA. Large-scale natural gradient tracer test in sand and gravel, Cape Cod, Massachusetts, 2, Analysis of tracer moments for a nonreactive tracer. Water Resour Res 1988;27:911–24.
[14] Gelhar L, Welty C, Rehfeldt K. A critical review of data on field-scale dispersion in aquifers. Water Resour Res 1992;28:1955–74.
[15] Gutknecht D, Blaschke A, Heinecke U, Hütter T, Sengschmitt D, Steiner K-H, et al. Auswirkungen der Versickerung von biologisch gereinigtem Abwasser auf das Grundwasser. Tech. rep., Institute of Hydraulic Engineering and Water Resources Management, Vienna University of Technology; 2002.
[16] Gutknecht G, Blaschke A, Herndl G, Reichel G, Schmalfuss R, Sengschmitt D, et al. Kolmationsprozesse am Beispiel des Stauraumes Freudenau. Tech. rep., Institute of Hydraulic Engineering and Water Resources Management, Vienna University of Technology, 1996.
[17] Ingendahl D. Dissolved oxygen concentration and emergence of sea trout fry from natural redds in tributaries of the river rhine. J Fish Biol 2001;58:325–41.
[18] Kinzelbach W. Numerische Methoden zur Modellierung des Transports von Schadstoffen im Grundwasser. München Wien: R. Oldenbourg Verlag; 1987.
[19] Lewandowski J, Nützmann G. Surface water–groundwater interactions: hydrological and biogeochemical processes at the lowland river Spree (Germany). In: Abesser C,

Wagener T, Nützmann G, editors. Groundwater–surface water interaction: process understanding, conceptualization and modelling. Perugia, Italy: IAHS, International association of hydrological sciences (IAHS); 2008. p. 30–8.
[20] Lu C, Kitanidis PK, Luo J. Effects of kinetic mass transfer and transient flow conditions on widening mixing zones in coastal aquifers. Water Resour Res 2009;45.
[21] McWhorter DB, Sunada DK. Ground-water hydrology and hydraulics. Water Resources Publications (Fort Collins, Colo.); 1977.
[22] Mucha I, Rodák D, Hlavatý Z, Banský L. Groundwater quality processes after bank infiltration from the Danube at Cunovo. Kluwer Academic Publishers; 2002. p. 177–220.
[23] Niederreiter R, Steiner K-H. Der Frost–Platten-Sammler (FPS) - ein neues korngrößenunabhängiges Verfahren zur Entnahme gefügeintakter oberflächennaher Urproben aus wassergesättigten Lockersedimenten (The Freeze-Panel-Sampler - an innovative method for taking undisturbed probes near to the surface of saturated, unconsolidated sediments). Hydrologie und Wasserbewirtschaftung 1999;43:30–2.
[24] Peyrard D, Sauvage S, Vervier P, Sanchez-Perez J, Quintard M. A coupled vertically integrated model to describe lateral exchanges between surface and subsurface in large alluvial floodplains with a fully penetrating river. Hydrol Process 2008;22:4257–73.
[25] Promny, M., 2007. Zur Advektion und Dispersion von Geschiebe. Ph.D. thesis, Institut für Wasserwesen, Universität der Bundeswehr München.
[26] Robinson C, Brovelli A, Barry D, Li L. Tidal influence on BTEX biodegradation in sandy coastal aquifers. Adv Water Resour 2009;32:16–28.
[27] Robinson C, Gibbes B, Li L. Driving mechanisms for groundwater flow and salt transport in a subterranean estuary. Geophys Res Letters 2006;33:1–4.
[28] Schaap MG, Leij FJ, Van Genuchten MT. ROSETTA: a computer program for estimating soil hydraulic parameters with hierachical pedotransfer functions. J Hydrol 2001;251:163–76.
[29] Storey R, Howard K, Williams D. Factors controlling riffle-scale hyporheic exchange flows and their seasonal changes in a gaining stream: a three-dimensional groundwater flow model. Water Resour Res 2003;39(2):1034.
[30] Tritthart, M., 2005. Three-dimensional numerical modelling of turbulent river flow using polyhedral finite volumes. Ph.D. thesis, Institute of Hydraulic Engineering and Water Resources Management, Vienna University of Technology.
[31] van Genuchten M. Th. A closed-form equation for predicting the hydraulic conductivity of unsaturated soils. Soil Sci Soc Am J 1980;44:892–8.
[32] Voss CI, Provost AM. SUTRA — a model for saturated–unsaturated variable-density ground-water flow with solute or energy transport. Tech. Rep. Water-Resources Investigations Report 02-4231, Reston, Virginia; 2008.